

Inviscid instability of a unidirectional flow sheared in two transverse directions

Kengo Deguchi[†]

School of Mathematics, Monash University, Clayton, VIC 3800, Australia

(Received 22 February 2019; revised 12 June 2019; accepted 17 June 2019;
first published online 15 July 2019)

Linear inviscid stability of general unidirectional flows sheared in one transverse direction has long been investigated by numerous researchers using the Rayleigh equation. However, unlike the simple shear flow considered in this equation, most physically relevant unidirectional flows vary in two transverse directions. Here the inviscid instability of such flows is studied by the large-Reynolds-number limit asymptotic analysis. We derive an *a priori* necessary condition for the existence of a limiting neutral mode, and develop a new numerical method to accurately capture singular neutral modes.

Key words: high-speed flow, transition to turbulence, Navier–Stokes equations

1. Introduction

Our concern is with the inviscid limit of stability for unidirectional flow U varying in two cross-streamwise directions y and z . The inviscid stability has long been studied for a more restricted form of background flow $U(y)$ since the early days of modern theoretical fluid dynamics. Many standard fluid dynamics textbooks devote a section to analysing the Rayleigh equation

$$v_{yy} - \alpha^2 v - \frac{U_{yy}}{U - c} v = 0, \quad (1.1)$$

deduced from the two-dimensional Euler equations linearised around $U(y)$. For a given perturbation wavenumber α , the above equation and the boundary conditions (usually impermeability conditions are used on the walls) constitute a linear eigenvalue problem for a complex phase speed c . When c is purely real, namely when the (Fourier-transformed) perturbation velocity v is neutral, the equation has a regular singular point, whose nature is well understood (Lin 1945, 1955). Otherwise, a perturbation growing in time should exist, but this is possible only when $U(y)$ has at least one inflection point; this is the famous Rayleigh's inflection point theorem and can be obtained by multiplying v^* , the complex conjugate of v , with (1.1) and integrating it over the flow domain.

The generalisation of the above classical inviscid stability result to $U(y, z)$ is of enormous importance in describing a wide range of real-world flows such as

[†] Email address for correspondence: kengo.deguchi@monash.edu

those through non-circular pipes or over corrugated walls. However, there have been surprisingly few analytic results deduced for such a generalised problem. In the previous works by Hocking (1968), Goldstein (1976), Benney (1984), Henningson (1987), Hall & Horseman (1991) and Hall & Smith (1991), the linearised three-dimensional Euler equations are combined into a single equation for the pressure perturbation p :

$$\mathcal{A}p \equiv \left(\frac{p_y}{(U-c)^2} \right)_y + \left(\frac{p_z}{(U-c)^2} \right)_z - \alpha^2 \frac{p}{(U-c)^2} = 0. \quad (1.2)$$

More recently, Li (2011) rederived (1.2) and showed that Howard's semicircle theorem holds (this was also noted earlier by Benney (1984)), whilst he can obtain a necessary condition for instability only for a special form of U . The difficulty in showing the latter result for a more general U is that, when z dependence is present, (1.1) becomes two coupled equations for the two cross-streamwise velocity components (or toroidal and poloidal potentials), and thus a weighted integral of those equations produces some cross-terms of the two different perturbation quantities. In addition, it is not straightforward to derive Rayleigh's theorem in the pressure form; for example, even in the classical case, we cannot show the theorem by the integration of $p^* \mathcal{A}p$ over the entire flow domain.

It is also widely acknowledged that, for the neutral case, the numerical computation of (1.2) is very challenging because of the singularity occurring on the critical curve where $U - c$ vanishes. Calculation of such a neutral solution is necessary in estimating the onset of the secondary instability of streamwise vortices occurring in curved and flat boundary layer flows (Hall & Horseman 1991; Yu & Liu 1991; Blackaby & Hall 1995; Li & Malik 1995; Andersson *et al.* 2001; Xu, Zhang & Wu 2017). In almost all previous studies, neutral modes were produced by solving the linearised Navier–Stokes equations at large Reynolds numbers rather than (1.2). The only exceptions are Andersson *et al.* (2001) and Hall (2018), who computed neutral solutions of (1.2) for a specific form of U .

The amplified instability wave modifies the mean streamwise vortex flow through the Reynolds stress and hence a closed-loop nonlinear interaction is formed. The origin of the theoretical framework of the loop interaction known to date can be traced back to Benney (1984). Hall & Smith (1991) were the first to mathematically rationalise the interaction between the streamwise vortex and the wave. The neutral finite-amplitude wave is still governed by (1.2) and large-Reynolds-number matched asymptotic expansion was used to analyse the interaction occurring within the thin critical layer surrounding the singularity; see Brown *et al.* (1993) also. Some years later, in order to explain the bypass transition in plane Couette flow, Waleffe (1997) integrated the idea of the loop interaction and the dynamical systems theory through the steady solutions found by Nagata (1990) and Clever & Busse (1992). In the 'self-sustaining process' proposed by Waleffe (1997), the instability of the streak is explained by the viscous problem, although the viscous effect must formally be neglected almost everywhere under the large-Reynolds-number assumption used to deduce the process. As a result, the importance of the critical layer was not noted until Wang, Gibson & Waleffe (2007), where the Reynolds-number scaling of the steady solutions was investigated for the first time. Motivated by this numerical work, Hall & Sherwin (2010) were able to reproduce the large-Reynolds-number solutions by numerically solving the reduced problem obtained in the vortex–wave interaction theory by Hall & Smith (1991), but with (1.2) replaced by the linearised Navier–Stokes equations.

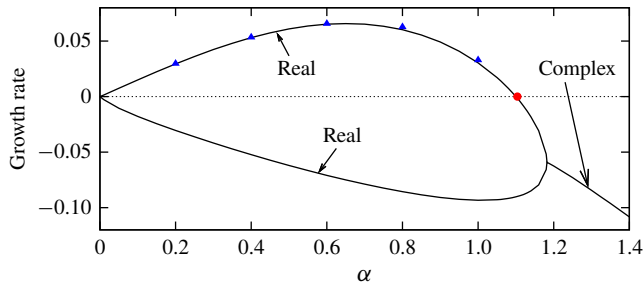


FIGURE 1. (Colour online) The growth rate associated with the streaky field of the nonlinear plane Couette flow solution. The solid curves are the linearised Navier–Stokes result computed in Deguchi & Hall (2016, figure 8a). The blue triangles are computed by applying the usual Chebyshev–Fourier spectrum method to the inviscid problem (1.2). In order to find the neutral point of this problem (the red circle), we must treat the singularity appropriately, as in § 3.1.

Subsequently, Deguchi & Hall (2016) theoretically and numerically studied the instability of the nonlinear steady solutions of plane Couette flow at large Reynolds numbers. Here we use the numerical result obtained in that paper to show the typical behaviour of the inviscid instability. The solid curves in figure 1 are the linearised Navier–Stokes result computed at the finite but large Reynolds number of 30 000. The background flow $U(y, z)$ is taken from the streamwise-averaged (streak) field of the nonlinear solution; the shape of the flow is qualitatively similar to the test profile (3.12) shown in figure 2. The blue triangles in figure 1 are the largest growth rate of solutions to (1.2) obtained by the Chebyshev–Fourier spectrum method (Li & Malik (1995) and Andersson *et al.* (2001) used the same method to compute the unstable modes, while Hall & Horseman (1991) used finite difference). As Lin (1955) explained in his book, the unstable mode of the inviscid problem represents the limiting eigenvalue of the viscous problem, whilst its complex conjugate might not describe the appropriate limit. The good agreement of the viscous and inviscid results here is certainly consistent with his comment. However, on approaching the neutral point the inviscid computation fails catastrophically, with many rogue eigenvalues. The reason for the failure is due to the singular nature of the inviscid solution at the critical level. With the standard spectrum or finite difference methods, such singular solutions are in general inaccessible; see Boyd (2001) for example.

We begin our analysis by formulating the stability problem in § 2. Some analysis of the classical Rayleigh equation is given in the same section to better explain our main idea. In § 3.1, we present our first discovery that, for neutral perturbation, we can actually derive a necessary condition for the existence of the neutral mode, if it describes the low-viscosity limit of the viscous problem. In § 3.2, we will establish a new accurate computational method to find neutral solutions of (1.2), using a novel combination of differential geometry and the method of Frobenius. The red circle in figure 1, which was unreachable using pre-existing methods, is computed by this new method. This, our second discovery, fills the last missing piece for the Reynolds-number-free computation of the vortex–wave interaction system. Finally, in § 4, we discuss our results briefly.

2. Formulation of the problem and review of the classical inviscid limit problem for $U(y)$

Our starting point is the Navier–Stokes equations linearised around the background flow $U(y, z)$ at the Reynolds number $R > 0$:

$$i\alpha u + v_y + w_z = 0, \quad i\alpha(U - c)u + U_y v + U_z w = -i\alpha p + R^{-1}(\Delta - \alpha^2)u, \quad (2.1a,b)$$

$$i\alpha(U - c)v = -p_y + R^{-1}(\Delta - \alpha^2)v, \quad i\alpha(U - c)w = -p_z + R^{-1}(\Delta - \alpha^2)w, \quad (2.1c,d)$$

where $\Delta = \partial_y^2 + \partial_z^2$. Here, note that, as usual, the velocity and pressure perturbations u, v, w, p are Fourier-transformed. The no-slip conditions $u = v = w = 0$ are imposed at $y = \pm 1$ and periodicity of the flow is assumed in z for the sake of simplicity; however, the discussion in § 3 holds for more complicated geometry with a straightforward extension. In this paper, we assume that the base flow U is differentiable to arbitrary order with respect to y and z . For large Reynolds numbers, the viscous terms may be neglected in the majority of the flow, and thus (1.2) holds. When the z dependence of the flow is absent, the pressure equation (1.2) is of course equivalent to the Rayleigh equation (1.1).

Here, before we begin the analysis of (1.2), we recall some properties of the classical Rayleigh equation in the pressure form to highlight our main idea (Tollmien 1935; Lin 1945, 1955). For the neutral case, the equation possesses a regular singular point at $y = y_c$, where $U - c$ vanishes. In a new coordinate, $n = y - y_c$, the singular point is simply $n = 0$. For small n , by assumption, the background flow has a regular expansion

$$U = \lambda_1 n + \lambda_2 n^2 + \dots, \quad (2.2)$$

whilst the Frobenius method can be used to show that the solution p is the sum of one regular function and another, multiplied by $n^3 \ln |n|$. The general solution must contain two free constants to satisfy the two boundary conditions at $y = \pm 1$. However, those constants in general differ for $n > 0$ and $n < 0$, because the solution is disconnected by the singularity at $n = 0$.

Formally, the possible jumps occurring in those constants must be fixed by considering the inner asymptotic expansion of (2.1) at the limit of large Reynolds number. Classical argument shows that viscosity is actually not negligible in a layer of $O(R^{-1/3})$ thickness around $n = 0$. The use of the stretched coordinate allows us to construct a smooth analytic solution within that critical layer. The matching of the inner and outer solutions is possible only when the outer general solution has the Frobenius form,

$$p = an^3 \tilde{f}(n) + b\{\mu n^3 \mathcal{L}(n) \tilde{f}(n) + \tilde{g}(n)\}, \quad \mu = -\frac{2\lambda_2 \alpha^2}{3\lambda_1}, \quad (2.3a,b)$$

where \tilde{f} and \tilde{g} have a regular expansion around $n = 0$, a and b are free constants, and the jump is absorbed into the modified logarithmic function

$$\mathcal{L}(n) = \begin{cases} \ln n, & \text{if } n > 0, \\ \ln |n| + i\theta, & \text{if } n < 0. \end{cases} \quad (2.4)$$

Here, we make a few remarks on the real constant θ , which physically describes the phase shift of the wave across the critical layer. Tollmien (1935) was the first

to derive (2.3) with $\theta = \pm\pi$; he began his analysis from the Frobenius solution for positive n and then extended it to negative n , choosing the branch cut of $\ln n$ in the complex plane. Lin (1955) called these multiple possibilities for the neutral solution a ‘mathematical dilemma’ in his book, showing that they came from the limit of small growth rate of the amplifying and damping modes. Those modes must simultaneously occur in the Rayleigh equation as a pair of complex conjugates, reflecting the fact that the ideal flow has time reversal symmetry. The asymptotic analysts, including Lin, then noticed that matching to the critical layer solution is possible only when

$$\theta = -\pi \operatorname{sgn}(U_n|_{n=0}). \tag{2.5}$$

This is in fact the place where the viscous effect breaking the time symmetry enters the analysis. The full spectral theory of (1.1) is complicated, especially because of the existence of a continuous spectrum associated with the singularity (see Balmforth & Morrison 1995; Hirota, Morrison & Hattori 2014; and references therein). However, if we are interested in the high-Reynolds-number asymptotic approximation of the viscous eigenvalue problem (2.1), whenever a singularity happens in the inviscid solution, we must look into the local viscous flow there. The consistency to the local viscous problem ensures that the approximated solution is the low-viscosity limit of the viscous problem and, more importantly, it excludes the complication of the inviscid spectrum.

Upon substituting (2.3) into the Rayleigh equation, we can find an equation for \tilde{f} and another equation for \tilde{f} and \tilde{g} . Those equations are second-order singular equations, but if we require regularity for \tilde{f} and \tilde{g} , the solutions are determined uniquely up to unknown amplitudes. Those amplitudes are absorbed into the constants a and b , so usually the values of \tilde{f} and \tilde{g} at $n = 0$ are normalised to unity. The two unknown constants a and b are fixed by the boundary condition on the walls, namely $p_y = 0$, which ensures $v = 0$ there. Those two conditions can be written in the matrix form $\mathbf{M}[a, b]^T = \mathbf{0}$ with 2×2 matrix \mathbf{M} computed by \tilde{f} and \tilde{g} . In order to have a non-trivial solution, $\det \mathbf{M}(\alpha, c) = 0$ must be satisfied. The neutral mode can be found at particular (α, c) , which makes the real and imaginary parts of the determinant vanish. This procedure has been used in the past two decades to find the singular solutions in shear flows; see Wu & Cowley (1995) and Deguchi & Walton (2018) for examples.

Now, suppose there is one critical layer in the flow. Since \tilde{f} and \tilde{g} are real functions, it is easy to see that the imaginary parts of the matrix \mathbf{M} come from the logarithmic function (2.4), which is multiplied by λ_2 in (2.3). Thus, in this case, U must have an inflection point at the critical point (Lin 1945). The same conclusion can be obtained by considering the integral

$$0 = \int_{\Omega} (p^* \mathcal{A} p - \text{c.c.}) \, d\Omega, \tag{2.6}$$

where Ω is the entire flow domain excluding the critical layer. Since p_y must vanish on the walls, the right-hand side becomes

$$\int_{\Omega} \partial_y \left(\frac{p^* p_y - p p_y^*}{U^2} \right) \, dy = \left[\frac{p^* p_y - p p_y^*}{U^2} \right]_{n=0+}^{0-} = -\frac{4i\alpha^2 \lambda_2 \theta}{\lambda_1^3} |b|^2 = \frac{4i\pi\alpha^2 U_{nm} |p|^2}{|U_n|^3} \Big|_{n=0}, \tag{2.7}$$

using the coefficient of $n^3 \ln |n|$ in the Frobenius expansion (2.3) and θ in (2.5).

We can further extend the above results for multiple critical layer cases. At each critical layer, we can define a local coordinate n . Thus, any neutral solution must satisfy

$$0 = \sum \left(\frac{U_m |p|^2}{|U_n|^3} \right) \Big|_{n=0}, \tag{2.8}$$

where the summation means that we collect the contributions from all the critical layers. If U_{yy} does not change its sign in $y \in [-1, 1]$, then p must vanish at the critical layers. However, this means that we must completely switch off b in the general solutions, and hence one of the boundary conditions is not satisfied.

Therefore, U_{yy} must change sign somewhere in order to have a neutral mode. This result, which is true only when the neutral mode is the proper large-Reynolds-number limit of (2.1), is not mathematically identical to that by Rayleigh, who studied the existence of the imaginary part of c . Nevertheless, in practice, both results can be used to preclude the presence of the unstable mode of inviscid origin for non-inflectional high-Reynolds-number flows. It is known that for large enough α ultimately there should be no unstable mode in the viscous problem, meaning that any unstable eigenvalue approaching the inviscid limit must pass through the neutral point at some critical value of α ; see figure 1, Drazin & Reid (1981). The cutoff value of α is typically $O(R^0)$, when the shear layer has a finite thickness.

Note that, even when the possibility of the inviscid instability is excluded, this does not mean that there is no instability in the flow. The condition here does not say anything about viscous instabilities (e.g. Tollmien–Schlichting wave), or some other instabilities only existing in a finite interval of Reynolds number.

3. The inviscid limit problem for $U(y, z)$

3.1. Necessary condition for existence of a neutral mode

The difficulty in analysing the neutral mode of the generalised Rayleigh equation (1.2) is that the singularity now occurs on a curve rather than a point. Thus, it is convenient to work in the body-fitted coordinates (n, s) attached to the critical curve (Slattery 1999). Here, we denote the length measured along straight lines that are normal to the critical curve $y = h(z)$ as n , and the arclength measured along the curve as s . Deguchi & Hall (2016) showed that the body-fitted coordinates version of (1.2) is

$$\frac{\partial^2 p}{\partial n^2} + \frac{\chi}{\mathcal{G}} \frac{\partial p}{\partial n} + \frac{1}{\mathcal{G}^2} \frac{\partial^2 p}{\partial s^2} - \frac{\chi' n}{\mathcal{G}^3} \frac{\partial p}{\partial s} - \alpha^2 p - \frac{2}{U} \left(\frac{\partial U}{\partial n} \frac{\partial p}{\partial n} + \frac{1}{\mathcal{G}^2} \frac{\partial U}{\partial s} \frac{\partial p}{\partial s} \right) = 0, \tag{3.1}$$

where $\mathcal{G} = 1 + \chi n$ and $\chi(s)$ is the signed curvature of the critical curve,

$$\chi(s) = - \frac{h_{zz}}{(1 + h_z)^{3/2}} = \frac{U_{zz} U_y^2 - 2U_{yz} U_y U_z + U_{yy} U_z^2}{U_n^3} \Big|_{n=0}. \tag{3.2}$$

For small n the base flow expands:

$$\left. \begin{aligned} U &= \lambda_1(s)n + \lambda_2(s)n^2 + \dots, & \lambda_1 &= U_n|_{n=0}, \\ \lambda_2 &= \frac{U_{yy} U_y^2 + 2U_{yz} U_y U_z + U_{zz} U_z^2}{2U_n^2} \Big|_{n=0}, \end{aligned} \right\}. \tag{3.3}$$

The benefit of using the body-fitted coordinates is that the Frobenius expansion is simply

$$p = p_0(s) + p_2(s)n^2 + p_{3L}(s)n^3 \mathcal{L}(n) + p_3(s)n^3 + \dots \tag{3.4}$$

The flow within the curved nonlinear critical layer was analysed by Wundrow & Goldstein (1994), where it was found that the logarithmic phase shift is a function of the wave amplitude. When the amplitude is small, the phase shift merely becomes the classical one (2.5), as shown in appendix A.

Substitution of (3.4) into (3.1) yields

$$p_2(s) = \frac{1}{2} \left\{ p_0'' - 2 \frac{\lambda_1'}{\lambda_1} p_0' - \alpha^2 p_0 \right\}, \quad p_{3L}(s) = \frac{\lambda_1^2}{3} \{ B_+ p_0'' + B_+' p_0' - \alpha^2 B_- p_0 \}, \tag{3.5a,b}$$

where, using the local Cartesian coordinates (n, \hat{s}) attached to the critical curve,

$$B_{\pm}(s) = \frac{2\lambda_2 \pm \lambda_1 \chi}{\lambda_1^3} = \frac{U_{nn} \pm U_{\hat{s}\hat{s}}}{U_n^3} \Big|_{n=0}. \tag{3.6}$$

Here, the expression for p_{3L} is significantly simplified from that in Deguchi & Hall (2016). This is the key to finding the necessary condition for the existence of a neutral mode. Assuming that there is one critical layer in the flow, and that the perturbation has periodicity in s , the right-hand side of (2.6) can be calculated as

$$\left[\oint \frac{p^* p_n - p p_n^*}{U^2} ds \right]_{n=0+}^{0-} = -2i\theta \oint (B_+ |p_0'|^2 + \alpha^2 B_- |p_0|^2) ds. \tag{3.7}$$

Here the integral is taken over one period in s . For the flows with multiple critical layers, summing up all the contributions, we find that any neutral perturbation must satisfy

$$0 = \sum \oint \left(\frac{(U_{nn} + U_{\hat{s}\hat{s}}) |p_s|^2 + (U_{nn} - U_{\hat{s}\hat{s}}) \alpha^2 |p|^2}{|U_n|^3} \right) ds \Big|_{n=0}, \tag{3.8}$$

which indeed has a generalised form of (2.8). Therefore, the necessary condition is that $U_{nn}^2 - U_{\hat{s}\hat{s}}^2 \leq 0$ is satisfied somewhere along an isocontour of U , or equivalently

$$(\Delta U) \{ 4U_{yz} U_y U_z + (U_{yy} - U_{zz})(U_y^2 - U_z^2) \} \leq 0, \tag{3.9}$$

holds somewhere in the flow, using (3.2), (3.3) and (3.6).

3.2. How to numerically solve (1.2) for neutral eigenfunction

In this section, we assume that there is one critical layer in the flow. For the classical case, there is no singularity at all, as seen in § 2. By analogy, regularity of the perturbation was assumed in Brown *et al.* (1993) and Blackaby & Hall (1995), but that assumption actually leads to some mathematical inconsistency, as shown in Deguchi & Hall (2016). The only exception occurs when the background flow is inflectional ($\lambda_2 = 0$) at the flat critical layer ($\chi = 0$). In this case, p_{3L} vanishes identically so there is no singularity in the solution; recently, Hall (2018) numerically solved (1.2) for this case. However, unlike the classical case, in general the neutral solution of (1.2) possesses a singularity since the condition (3.8) is not as restrictive

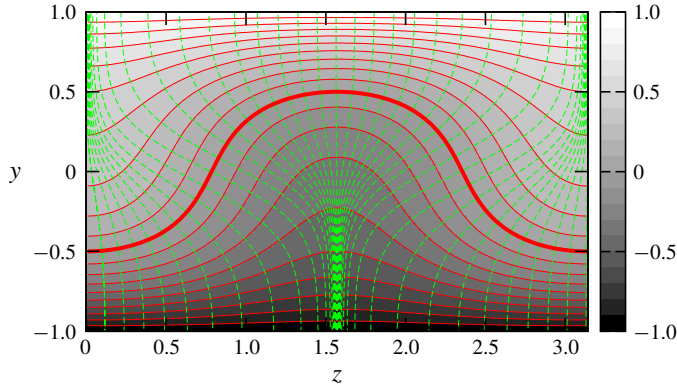


FIGURE 2. (Colour online) The model flow profile (3.12). The red solid curves are the isocontour of U , and hence η is constant along this curve (the thick curve is the critical level for the steady mode). The green dashed curves are plotted fixing ζ .

as the classical case. Andersson *et al.* (2001) computed singular neutral modes assuming that U only contains zeroth and first Fourier harmonics in z . In this specific case, the singularities of the Fourier-transformed equation are identified analytically, and hence the equation can be integrated in the complex y plane.

In our methodology, to handle general U , the singularity is treated in the physical space using curved coordinates. However, the use of the body-fitted coordinates is not desirable for the global numerical analysis because it may break down as we move away from the critical curve. Thus, here we consider other more useful curvilinear coordinates (η, ζ) , which we hereafter refer to as flow-fitted coordinates. The idea here is to use $U - c = \eta$ as one of the coordinates to transform all the critical curves and walls to straight lines; a similar coordinate was used in Goldstein (1976) and Wundrow & Goldstein (1994) to study the flow near the critical curve. For the other coordinate, $\zeta(y, z)$, we require the orthogonality condition

$$\eta_y \zeta_y + \eta_z \zeta_z = 0. \tag{3.10}$$

Then the standard differential geometry theory (see appendix B) can be used to show that $y(\eta, \zeta)$ and $z(\eta, \zeta)$ are found by integrating

$$y_\eta = \frac{\eta_y}{\eta_y^2 + \eta_z^2}, \quad \text{and} \quad z_\eta = \frac{\eta_z}{\eta_y^2 + \eta_z^2}, \tag{3.11a,b}$$

in η . Some initial conditions are needed for these differential equations: here we assume that ζ is the arclength of the critical level $\eta = 0$. Figure 2 shows the isocontour of η, ζ for the simple model profile

$$U(y, z) = y + (1 - y^2) \frac{\cos(2z) - 2y}{3}. \tag{3.12}$$

We shall shortly use this model profile (having a period π in z) to test the new method.

The generalised Rayleigh equation (1.2) in the flow-fitted coordinates is

$$p_{\eta\eta} - 2\eta^{-1}p_\eta + Ap_\eta + 2\mathcal{E}p_{\zeta\zeta} + \mathcal{E}_\zeta p_\zeta - \alpha^2\Theta p = 0, \tag{3.13}$$

where the coefficients $\Theta = (\eta_y^2 + \eta_z^2)^{-1}$, $\Lambda = \Theta \Delta \eta$ and $\mathcal{E} = (y_\eta/z_\zeta)^2/2$ are computable since $y(\eta, \zeta)$ and $z(\eta, \zeta)$ are known (the detail of the transformation is given in appendix B). The flow-fitted coordinates analogue of the Frobenius form is

$$p(\eta, \zeta) = \eta^3 f_a(\eta, \zeta) + \{\eta^3 \mathcal{L}(\eta) f_b(\eta, \zeta) + g(\eta, \zeta)\}. \tag{3.14}$$

Then, substituting (3.14) into (3.13), and assuming f_a and (f_b, g) are independent, after some algebra, we obtain

$$f_{\eta\eta} + 4\eta^{-1} f_\eta + \Lambda(f_\eta + 3\eta^{-1} f) + 2\mathcal{E} f_{\zeta\zeta} + \mathcal{E}_\zeta f_\zeta - \alpha^2 \Theta f = 0, \tag{3.15a}$$

$$g_{\eta\eta} - 2\eta^{-1} g_\eta + \Lambda g_\eta + 2\mathcal{E} g_{\zeta\zeta} + \mathcal{E}_\zeta g_\zeta - \alpha^2 \Theta g + 2\eta^2 f_{b\eta} + (\Lambda\eta + 3)\eta f_b = 0. \tag{3.15b}$$

Here, both f_a and f_b satisfy the first equation and thus we neglect the subscripts. The regular solutions of equations (3.15) must have the small- η expansions

$$f = f_0(\zeta) + f_1(\zeta)\eta + O(\eta^2), \quad g = g_0(\zeta) + g_2(\zeta)\eta^2 + O(\eta^4), \tag{3.16a,b}$$

where from a straightforward calculation

$$f_1 = -\frac{3\Lambda}{4} f_0, \quad g_2 = \frac{1}{2} \{2\mathcal{E} g_0'' + \mathcal{E}_\zeta g_0' - \alpha^2 \Theta g_0\}, \quad f_{b0} = \mu_2 g_0'' + \mu_1 g_0' + \mu_0 \alpha^2 g_0, \tag{3.17a-c}$$

$$\mu_2 = -\frac{2(\Lambda\mathcal{E} + \mathcal{E}_\eta)}{3}, \quad \mu_1 = -\frac{(\Lambda\mathcal{E}_\zeta + \mathcal{E}_{\eta\zeta})}{3}, \quad \mu_0 = \frac{(\Lambda\Theta + \Theta_\eta)}{3}. \tag{3.17d-f}$$

Those requirements act as ‘initial conditions’ of the differential equations (3.15) at $\eta = 0$. Hence, for given f_{0a} and g_0 , the solutions f_a, f_b and g for $\eta > 0$ and $\eta < 0$ are uniquely determined.

The degrees of freedom f_{0a} and g_0 left in the general solution are exactly what we need to satisfy the boundary conditions on the walls. This point becomes clear in the Fourier-expanded forms $f_{0a}(\zeta) = \sum_m a_m e^{im\beta\zeta}$ and $g_0(\zeta) = \sum_m b_m e^{im\beta\zeta}$, assuming the periodicity of the flow in ζ ; here β is the ‘wavenumber’ fixed from the arclength of the critical curve. The solution of (3.15a) can be found by integrating the equation in η from $\eta = 0$ (or successively determining the coefficients of the local expansion) using initial data f_0 ; we write such a solution as $f = \tilde{f}(\eta, \zeta; f_0)$. Then, if we use f_{0a} as the initial condition, from the linearity of the problem

$$f_a = \tilde{f}(n, \zeta; f_{0a}) = \tilde{f}\left(n, \zeta; \sum_m a_m e^{im\beta\zeta}\right) = \sum_m a_m \tilde{f}(n, \zeta; e^{im\beta\zeta}). \tag{3.18}$$

This means that we can expand f_a using the canonical basis solutions of (3.15a) computed by the initial monochromatic Fourier modes. Likewise, for given g_0 , we can integrate (3.15b) to find $\tilde{g}(\eta, \zeta; g_0)$, noting that f_b in the equation can be obtained by applying the initial condition (3.17) to \tilde{f} . Finally, using those expressions of f_a, f_b and g in (3.14), we get the expression of p that is analogous to (2.3):

$$p = \sum_m a_m \eta^3 \tilde{f}(\eta, \zeta; e^{im\beta\zeta}) + b_m \{\eta^3 \tilde{f}(\eta, \zeta; \mu^{(m)} e^{im\beta\zeta}) \mathcal{L}(\eta) + \tilde{g}(\eta, \zeta; e^{im\beta\zeta})\}. \tag{3.19}$$

Here $\mu^{(m)} = -m^2 \beta^2 \mu_2 + im\beta \mu_1 + \mu_0$ can be found from (3.17). The requirement that all the Fourier modes of p_η must vanish on the walls yields the algebraic linear

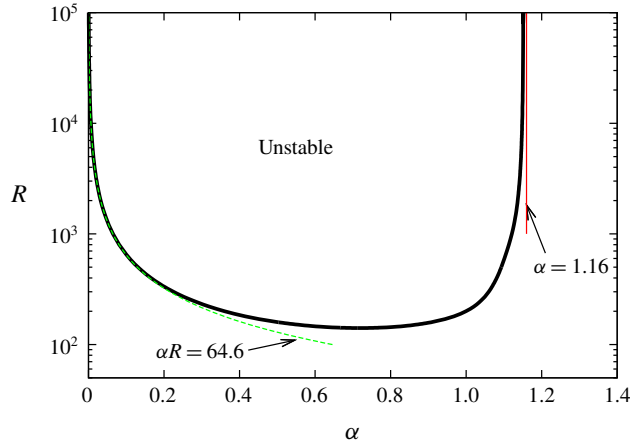


FIGURE 3. (Colour online) The model flow (3.12) becomes unstable above the thick black solid curve according to the linearised Navier–Stokes equations (2.1). The red solid line is the neutral inviscid limit solution found by (1.2). The green dashed curve is the long-wavelength asymptotic limit. Approximately 200 collocation points are used in $\eta \in [-1, 1]$, whilst 35 Fourier harmonics are used for ζ .

problem $\mathbf{M}[a_m, b_m]^T = 0$. The neutral values of α and c can in principle be found by $\det \mathbf{M}(\alpha, c) = 0$ as in the classical case.

Here, we demonstrate how to find the neutral mode of (1.2) for the model flow profile (3.12). As remarked in § 1, this profile is qualitatively similar to the streak field of the steady nonlinear solutions of plane Couette flow, but the explicit simple form of the model makes the test problem more tractable. From the condition derived in § 3.1, there might be instability in this flow. The full neutral curve of this profile can indeed be found as shown in figure 3. The asymptotic limit of the left-hand branch can easily be found, as it has the same scaling as that discussed in Deguchi *et al.* (2013) and thus has a regular limit. In contrast, the inviscid limit approximating the right-hand branch is the singular limit and hence we need a much more complicated analysis. The most unstable mode is steady ($c = 0$) and has symmetries $p(y, z) = -p^*(-y, z + L_z/2) = -p(y, -z)$ (see figure 4); here we focus only on this mode for the sake of simplicity. The existence of the steady mode is another benefit to using (3.12) for the test purpose.

In theory, we can first compute the canonical basis functions such as $\tilde{f}(n, \zeta; e^{im\beta\zeta})$ by numerically solving (3.15), and then seek the special value of α that makes the matrix \mathbf{M} singular; alternatively, we can treat α^2 as an eigenvalue, as we shall see shortly. However, it turns out that the canonical basis solutions typically take very large values near the walls at $\eta = \pm 1$, and hence using them in the entire domain leads to numerical inaccuracy. Therefore, it is more sensible to use the canonical basis functions only for $|\eta| < \eta_0$, where we choose $\eta_0 = 0.2$ for the model profile. As long as $\eta_0 > 0$ is chosen to be not too large, the canonical basis functions behave well and any fine tuning is unnecessary here.

For $|\eta| > \eta_0$, the usual Chebyshev collocation method can be employed to solve (3.13). In this outer zone, the pressure p is determined by the spectral coefficients $\varphi_{m,l}$ multiplied by the l th Chebyshev polynomials and the m th Fourier harmonics. At $\eta = \pm\eta_0$, we require that p and p_η are continuous. The unknowns associated

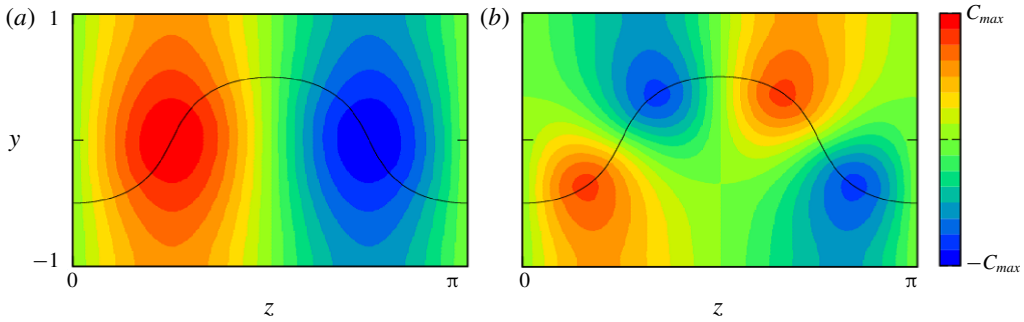


FIGURE 4. (Colour online) The pressure eigensolution on the right-hand branch of the full neutral curve in figure 1, for $R=10\,000$. Panels (a) and (b) are the real part ($C_{max}=1$) and the imaginary part ($C_{max}=0.2$), respectively. The black solid curve is the critical curve.

with those conditions are, of course, a_m and b_m , which fixes p within the inner zone $|\eta| < \eta_0$. Evaluating (3.13) at the suitable collocation points, together with the boundary conditions on the walls, and the continuity of p and p_η , we have an eigenvalue problem

$$\mathbf{M}_1 \begin{bmatrix} a_m \\ b_m \\ \varphi_{m,l} \end{bmatrix} = \alpha^2 \mathbf{M}_2 \begin{bmatrix} a_m \\ b_m \\ \varphi_{m,l} \end{bmatrix}, \tag{3.20}$$

which can, for example, be solved by the LAPACK routine. (Note that (3.13), (3.15) and (3.17) can be separated into the part proportional to α^2 and the rest.) Here, as usual, the unphysical eigenvalues associated with the boundary conditions must be removed (see Boyd 2001). For more general flows, we must assume the value of c to compute the flow-fitted coordinates. If a positive purely real value cannot be found in the eigenvalues α^2 , the computation must be repeated varying c .

For the steady mode of the model flow (3.12), this iteration is not necessary, and the numerical result indeed predicts the critical value $\alpha = 1.16$, at which the right-hand branch of the full neutral curve tends to $R \rightarrow \infty$ (figure 3). The comparison of the pressure eigenmodes shown in figure 5 also confirms that the solution of the limiting inviscid problem indeed provides excellent predictions for the full linear Navier–Stokes result. In figure 3 we also note that for the left-hand branch viscosity is not negligible everywhere, because the small critical wavenumber of $O(R^{-1})$ ensures the viscous–convective balance.

4. Conclusion

The inviscid limit of the linear instability occurring in a unidirectional shear flow sheared in two transverse directions has been studied. The sufficient condition for the existence of a neutral mode is given in §3.1. The new numerical method developed in §3.2 led us to the first accurate numerical computation of singular neutral modes.

The new numerical method is tested against the simple model flow (3.12) in §3. The model flow has a similar shape to the streak field of the steady nonlinear plane Couette solution used in figure 1. Thus not surprisingly the same methodology can be used to produce the red circle in figure 1. Again, the result is consistent with the large-Reynolds-number computation based on the linearised

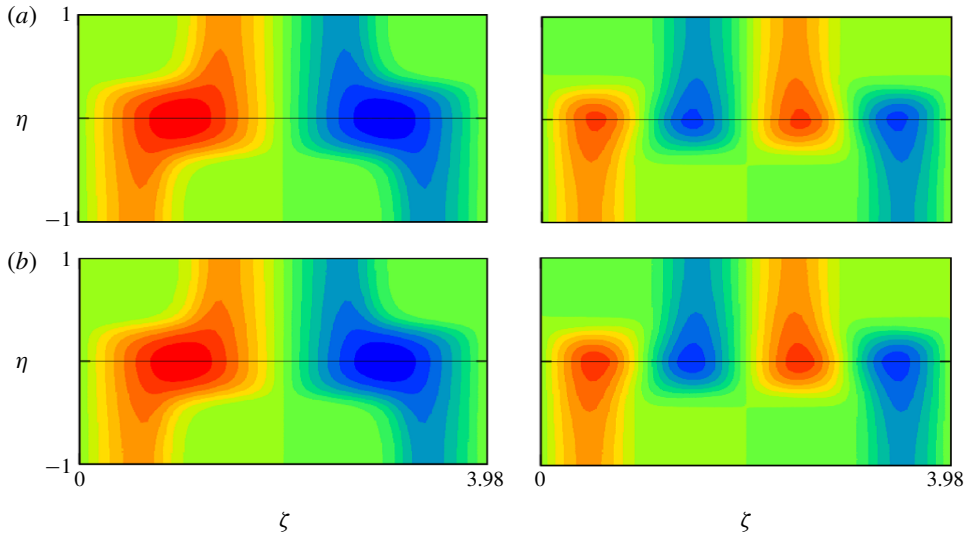


FIGURE 5. (Colour online) (a) The same results as figure 4, but plotted in the (η, ζ) coordinates. (b) The inviscid solution obtained by applying the new method to (1.2). This result corresponds to the red line in figure 3.

Navier–Stokes equations. In the vortex–wave interaction framework, this neutral mode is exactly the one maintaining the steady roll streak. Therefore, the accurate computation of it is indispensable to completely remove the Reynolds-number (or the regularisation-parameter) dependence from the asymptotically reduced system. The delicate singular structure is also important in estimating the stability of the solution, as shown by Deguchi & Hall (2016). The importance of the singular neutral solution of (1.2) is not limited to purely hydrodynamic problems; see the vortex–wave interaction theory formulated for weakly stratified flows by Deguchi (2017) and Olvera & Kerswell (2017). Moreover, it was recently shown by Deguchi (2019) that it appears as a part of the self-sustained magnetohydrodynamic dynamo process at large Reynolds numbers.

The proposed algorithm can be utilised for quite general background flows as long as the critical layers do not intersect each other (i.e. the shear does not vanish along the critical level). An interesting case is the generalised Couette flow between wavy walls. In this case, since $\Delta U = 0$ is satisfied, η and ζ are harmonic functions and can be found analytically. The method can also be used for non-circular pipe flows, or more complicated forced flows with many critical layers. In the latter case, complication of the numerical code may be unavoidable, but a general code could be developed by combining the local basis around the critical layer constructed here and the spectral/hp method (Karniadakis & Sherwin 2005).

It should also be remarked that the new method is more numerically economical than the large-Reynolds-number computation of the linearised Navier–Stokes equations, where the three velocity components and the pressure (or two potentials) must be solved. Near the critical level, the amplitude of the perturbation velocity behaves like n^{-1} , and this singular behaviour must be reconciled within the critical layer of thickness $R^{-1/3}$. The bottleneck of the stability analysis is the algebraic linear eigenvalue problem part because the high resolution required to resolve the asymptotically sharp flow structure makes the stability matrix huge. On the other hand,

here we solve a single equation for the pressure, and no sharp structure appears when it is converted to the Frobenius form.

Acknowledgements

This work is supported by Australian Research Council Discovery Early Career Researcher Award DE170100171. The author acknowledges the anonymous referees who carefully checked the equations and grammatical errors, and gave many helpful comments that significantly improved the clarity of this paper.

Appendix A. Critical layer analysis

Here we use the body-fitted coordinates. The flow inside the critical layer can be analysed by using the stretched variable $N = n/\delta$ with the critical layer thickness $\delta = R^{-1/3}$. As usual, here we omit the analysis of terms involving $\ln \delta$ (the terms of logarithmic order match automatically and hence do not need to be considered separately). The appropriate inner expansions are

$$\left. \begin{aligned} p &= P_0(s) + \delta^2 P_2(N, s) + \delta^3 P_3(N, s) + \dots, \\ u &= \delta^{-1} U_0(N, s) + U_1(N, s) + \dots, \\ (v, w) \cdot \mathbf{e}_n &= V_0(N, s) + \delta V_1(N, s) + \dots, \\ (v, w) \cdot \mathbf{e}_s &= \delta^{-1} W_0(N, s) + W_1(N, s) + \dots. \end{aligned} \right\} \tag{A 1}$$

In order to match the critical layer solution to the outer solution, P_0 , $N^{-2}P_2$, $N^{-3}P_3$, NU_0 , U_1 , V_0 , $N^{-1}V_1$, NW_0 and W_1 must tend to $O(N^0)$ quantities as $|N| \rightarrow \infty$. From the cross-streamwise components of (2.1), we can deduce the critical layer equations

$$\left. \begin{aligned} \mathcal{S}V_0 &= -P_{2N}, & \mathcal{S}V_1 + i\alpha\lambda_2 N^2 V_0 &= -P_{3N} + \chi V_{0N}, \\ \mathcal{S}W_0 &= -P'_0, & \mathcal{S}W_1 + i\alpha\lambda_2 N^2 W_0 &= \chi W_{0N}, \end{aligned} \right\} \tag{A 2}$$

where $\mathcal{S} = \{i\alpha\lambda_1 N - \partial_N^2\}$. The far-field behaviour of the functions V_0 , W_0 and W_1 must be consistent with those of P_0 and P_2 where there should be no jump according to the Frobenius expansion (3.4). Hence $[V_0, NW_0, W_1](N, s)$ tend to $[\widehat{V}_0, \widehat{W}_0, \widehat{W}_1](s)$ as $|N| \rightarrow \infty$. The jump may appear in V_1 , which is linked to P_3 . Using the streamwise component of the momentum equation and the continuity equation, the higher-order critical layer equations can be combined to yield

$$\mathcal{S}V_{1NN} = i\alpha\{2\lambda_2 V_0 + 2\lambda'_1(NW_1)_N + (2\lambda'_2 - \chi\lambda'_1)(N^2 W_0)_N + \chi\lambda_1(N^2 W_{0s})_N\} + H, \tag{A 3}$$

where $H(N, s) \rightarrow 0$ as $|N| \rightarrow \infty$. Therefore, the solution must have the form

$$\left. \begin{aligned} V_1 &= \frac{i\alpha\{2\lambda_2 \widehat{V}_0 + 2\lambda'_1 \widehat{W}_1 + (2\lambda'_2 - \chi\lambda'_1)\widehat{W}_0 + \chi\lambda_1 \widehat{W}'_0\}}{(\alpha|\lambda_1|)^{4/3}} F(\xi) + h(N, s), \\ \xi &= (\alpha|\lambda_1|)^{1/3} N, \end{aligned} \right\} \tag{A 4}$$

where $h(N, s) \rightarrow 0$ as $|N| \rightarrow \infty$ and $F(\xi)$ satisfies $\{i \operatorname{sgn}(\lambda_1)\xi - \partial_\xi^2\}F_{\xi\xi} = 1$. The asymptotic behaviour $-iF_\xi \rightarrow \mathcal{L}(\xi) + (\text{regular part})$ with $\theta = -\pi \operatorname{sgn}(\lambda_1)$ as $|\xi| \rightarrow \infty$ is well known in the asymptotic study of shear flow instability (see Lin 1955; Haberman 1972; Deguchi & Walton 2018; and references therein).

Appendix B. Property of the flow-fitted coordinates

The differentiation of a function ϕ in the (η, ζ) coordinates can be found by the chain rule as

$$\begin{bmatrix} \phi_\eta \\ \phi_\zeta \end{bmatrix} = \begin{bmatrix} y_\eta & z_\eta \\ y_\zeta & z_\zeta \end{bmatrix} \begin{bmatrix} \phi_y \\ \phi_z \end{bmatrix}. \tag{B 1}$$

If the determinant

$$J = y_\eta z_\zeta - y_\zeta z_\eta, \tag{B 2}$$

is non-vanishing, the inverse transformation can be obtained as

$$\begin{bmatrix} \phi_y \\ \phi_z \end{bmatrix} = \frac{1}{J} \begin{bmatrix} z_\zeta & -z_\eta \\ -y_\zeta & y_\eta \end{bmatrix} \begin{bmatrix} \phi_\eta \\ \phi_\zeta \end{bmatrix}. \tag{B 3}$$

Replacing ϕ by η or ζ in the above equations,

$$\eta_y = \frac{z_\zeta}{J}, \quad \zeta_y = -\frac{z_\eta}{J}, \quad \eta_z = -\frac{y_\zeta}{J}, \quad \zeta_z = \frac{y_\eta}{J}. \tag{B 4a-d}$$

Given the first derivatives (B 3), we can show that the two-dimensional Laplace operator becomes

$$\begin{aligned} \Delta\phi &= \frac{1}{J} \left\{ \left(\frac{y_\zeta^2 + z_\zeta^2}{J} \phi_\eta \right)_\eta + \left(\frac{y_\eta^2 + z_\eta^2}{J} \phi_\zeta \right)_\zeta \right\} \\ &= (\Delta\eta)\phi_\eta + (\Delta\zeta)\phi_\zeta + (\eta_y^2 + \eta_z^2)\phi_{\eta\eta} + (\zeta_y^2 + \zeta_z^2)\phi_{\zeta\zeta}. \end{aligned} \tag{B 5}$$

Here in order to calculate the second line we have used

$$\left. \begin{aligned} \zeta_y^2 + \zeta_z^2 &= \frac{y_\eta^2 + z_\eta^2}{J^2}, & \eta_y^2 + \eta_z^2 &= \frac{y_\zeta^2 + z_\zeta^2}{J^2}, \\ \Delta\eta &= \frac{1}{J} \left(\frac{y_\zeta^2 + z_\zeta^2}{J} \right)_\eta, & \Delta\zeta &= \frac{1}{J} \left(\frac{y_\eta^2 + z_\eta^2}{J} \right)_\zeta, \end{aligned} \right\} \tag{B 6}$$

found from (B 4) and the first line of (B 5). There is another set of useful formulae obtained by the chain rule:

$$\frac{\partial y}{\partial y} = \eta_y y_\eta + \zeta_y y_\zeta = 1, \quad \frac{\partial y}{\partial z} = \eta_z y_\eta + \zeta_z y_\zeta = 0, \tag{B 7a,b}$$

$$\frac{\partial z}{\partial y} = \eta_y z_\eta + \zeta_y z_\zeta = 0, \quad \frac{\partial z}{\partial z} = \eta_z z_\eta + \zeta_z z_\zeta = 1. \tag{B 7c,d}$$

Then (B 7) and (3.10) can be used to deduce (3.11) and $(y_\zeta, z_\zeta) = (\zeta_y, \zeta_z)/(\zeta_y^2 + \zeta_z^2)$. Finally, those relationships and (B 4) allow us to further simplify the Laplace operator through

$$\frac{\Delta\zeta}{\eta_y^2 + \eta_z^2} = \mathcal{E}_\zeta, \quad \frac{\zeta_y^2 + \zeta_z^2}{\eta_y^2 + \eta_z^2} = 2\mathcal{E}, \tag{B 8a,b}$$

and hence the transformed Rayleigh equation (3.13) is obtained.

REFERENCES

- ANDERSSON, P., BRANDT, L., BOTTARO, A. & HENNINGSON, D. S. 2001 On the breakdown of boundary layer streaks. *J. Fluid Mech.* **428**, 29–60.
- BALMFORTH, N. J. & MORRISON, P. J. 1995 Normal modes and continuous spectra. *Ann. N.Y. Acad. Sci.* **773**, 80–94.
- BENNEY, D. 1984 The evolution of disturbances in shear flows at high Reynolds numbers. *Stud. Appl. Maths* **70**, 1–19.
- BLACKABY, N. D. & HALL, P. 1995 The nonlinear evolution of the inviscid secondary instability of streamwise vortex structures. *Phil. Trans. R Soc. Lond. A* **352**, 483–502.
- BOYD, J. P. 2001 *Chebyshev and Fourier Spectral Methods*. Dover.
- BROWN, P. G., BROWN, S. N., SMITH, F. T. & TIMOSHIN, S. N. 1993 On the starting process of strongly nonlinear vortex/Rayleigh interactions. *Mathematika* **40**, 7–29.
- CLEVER, R. M. & BUSSE, F. H. 1992 Three-dimensional convection in a horizontal fluid layer subjected to a constant shear. *J. Fluid Mech.* **234**, 511–527.
- DEGUCHI, K. 2017 Scaling of small vortices in stably stratified shear flows. *J. Fluid Mech.* **821**, 582–594.
- DEGUCHI, K. 2019 High-speed shear driven dynamos. Part 1. Asymptotic analysis. *J. Fluid Mech.* **868**, 176–211.
- DEGUCHI, K. & HALL, P. 2016 On the instability of vortex–wave interaction states. *J. Fluid Mech.* **802**, 634–666.
- DEGUCHI, K. & WALTON, A. G. 2018 Bifurcation of nonlinear Tollmien–Schlichting waves in a high-speed channel flow. *J. Fluid Mech.* **843**, 53–97.
- DRAZIN, P. G. & REID, W. H. 1981 *Hydrodynamic Stability*. Cambridge University Press.
- GOLDSTEIN, M. E. 1976 *Aeroacoustics*. McGraw-Hill.
- HABERMAN, R. 1972 Critical layers in parallel flows. *Stud. Appl. Maths* **51**, 139–161.
- HALL, P. 2018 Vortex–wave interaction arrays: a sustaining mechanism for the log layer? *J. Fluid Mech.* **850**, 46–82.
- HALL, P. & HORSEMAN, N. 1991 The linear inviscid secondary instability of longitudinal vortex structures in boundary layers. *J. Fluid Mech.* **232**, 357–375.
- HALL, P. & SHERWIN, S. 2010 Streamwise vortices in shear flows: harbingers of transition and the skeleton of coherent structures. *J. Fluid Mech.* **661**, 178–205.
- HALL, P. & SMITH, F. T. 1991 On strongly nonlinear vortex/wave interactions in boundary-layer transition. *J. Fluid Mech.* **227**, 641–666.
- HENNINGSON, D. S. 1987 Stability of parallel inviscid shear flow with mean spanwise variation. *Tech. Rep. FFA-TN 1987–57*. Aeronautical Research Institute of Sweden.
- HIROTA, M., MORRISON, P. J. & HATTORI, Y. 2014 Variational necessary and sufficient stability conditions for inviscid shear flow. *Proc. R. Soc. Lond. A* **470**, 20140322.
- HOCKING, L. M. 1968 Long wavelength disturbances to non-planar parallel flow. *J. Fluid Mech.* **31** (4), 625–634.
- KARNIADAKIS, G. E. & SHERWIN, S. J. 2005 *Spectral/hp Element Methods for Computational Fluid Dynamics*, 2nd edn. Oxford University Press.
- LI, Y. 2011 Stability criteria of 3D inviscid shears. *Q. Appl. Maths* **69**, 379–387.
- LI, F. & MALIK, M. R. 1995 Fundamental and subharmonic secondary instabilities of Görtler vortices. *J. Fluid Mech.* **297**, 77–100.
- LIN, C. C. 1945 On the stability of two-dimensional parallel flows. Part III – stability in a viscous fluid. *Q. Appl. Maths* **3**, 277–301.
- LIN, C. C. 1955 *The Theory of Hydrodynamic Stability*. Cambridge University Press.
- NAGATA, M. 1990 Three-dimensional finite-amplitude solutions in plane Couette flow: bifurcation from infinity. *J. Fluid Mech.* **217**, 519–527.
- OLVERA, D. & KERSWELL, R. R. 2017 Exact coherent structures in stably stratified plane Couette flow. *J. Fluid Mech.* **826**, 583–614.
- SLATTERY, J. C. 1999 *Advanced Transport Phenomena*. Cambridge University Press.
- TOLLMIEEN, W. 1935 Ein allgemeines Kriterium der Instabilität laminarer Geschwindigkeitsverteilungen. *Nachr. Ges. Wiss. Göttingen* **1**, 79–114.

- WALEFFE, F. 1997 On a self-sustaining process in shear flows. *Phys. Fluids* **9**, 883–900.
- WANG, J., GIBSON, J. F. & WALEFFE, F. 2007 Lower branch coherent states: transition and control. *Phys. Rev. Lett.* **98**, 204501.
- WU, X. & COWLEY, S. J. 1995 On the nonlinear evolution of instability modes in unsteady shear layers: the Stokes layer as a paradigm. *Q. J. Mech. Appl. Maths* **48** (2), 159–188.
- WUNDROW, D. W. & GOLDSTEIN, M. E. 1994 Nonlinear instability of a uni-directional transversely sheared mean flow. *NASA TM* 106779.
- XU, D., ZHANG, Y. & WU, X. 2017 Nonlinear evolution and secondary instability of steady and unsteady Görtler vortices induced by free-stream vortical disturbances. *J. Fluid Mech.* **829**, 681–730.